Self-consistent analysis of the contact phenomena in low-mobility semiconductors

Yevgeni Preezant and Nir Tessler[a]
Department of Electrical Engineering, Technion–Israel Institute of Technology, Haifa 32000, Israel

Self-consistent solution of charge injection and charge transport in low mobility light emitting diodes (LEDs) is reported. We show that an explicit description of the contact region under the same premise as the transport equations is needed to accurately evaluate the current–voltage characteristics of polymer or small-molecule based LEDs. The results are compared to widely used models, which treat the contact region in an implicit manner. © *2003 American Institute of Physics.* [DOI: 10.1063/1.1539534]

I. INTRODUCTION

Charge injection and transport phenomena have been studied for many years and in many material systems[1] including organic semiconductors.[2–5] Many of these studies are now being revisited[4,6–10] as high quality devices seem to emerge through the use of new and better materials.[11] Lately, it has become evident that a better description of the contact region or the contact phenomena in organic-material based devices is required. It has been proposed that one may need to add interface states in the form of traps or dipoles to better simulate experimental results.[12,13] However, it has also been suggested that the contact phenomena in organic materials should be formulated in a manner adequate to describe low-mobility semiconductors[14,15] and not as a correction to contact phenomena in ceramic semiconductors. The common feature of all the models described above is that they treat contact phenomena separately or lump the contact region into a single point in space. Recently, a molecularly oriented transport model[16] that treats the contact region in an explicit manner was developed and applied to various light emitting diode (LED) structures. In this article we also make the contact region an explicit part of the device and solve the entire device using a single semiconductor device model. Moreover, we show that the effect of disorder and the Gaussian density of states (DOS) can be included in such a model in an easy to implement manner.

II. PHYSICAL PICTURE

Before describing the complete model we first examine the physical picture we use to describe the contact region. Investigation and development of physical models for charge injection into organic as well as disordered materials can be traced back several decades. A microscopic description of the charge injection process would generally include ballistic motion of the charge carrier through the polymer, energy loss and thermalization, and the hopping motion of thermalized carriers between the localization site to the collector or recombination at the source. However, a macroscopic semiconductor device model is generally applied to thermalized carriers only and hence if we want to include the contact region in such a model the thermalization length must be negligibly small. Thermalization of carriers in polymers can be described as ballistic motion of the particle under the influence of viscous drag force in the image potential field:[17]

$$m\frac{dv}{dt} = -e\frac{v}{\mu} - e\frac{d\varphi}{dx},\qquad(1)$$

which lead to an approximate expression for the thermalization distance for hot carriers:

$$x_t \approx \mu v_0 (m/e),\qquad(2)$$

where v_0 is the initial velocity of the injected carrier, μ is the mobility, and m is the carrier mass. This equation illustrates the relevance of the low mobility to the physical picture. Although the mass of a carrier polaron is not well known the overall thermalization length is believed to be in the range of 1–0.1 nm and hence one may assume that the carriers thermalize at the first-hop site:[15] and that any further motion of the carrier is governed by hopping transport in the electronic potential. This process can be modeled by Monte-Carlo simulation[15] or by the drift–diffusion equation.[17–19]

In the current context one should compare the thermalization length with the length associated with the contact region, defined as the space between the metal/semiconductor interface and the potential peak (see Fig. 1). The length of this contact region varies between $\sim$10 and $\sim$5 nm for applied voltages between 2.5 and 4 V, respectively (assuming a built-in voltage of 2 V and a 100 nm thick device). In the low applied voltage range (relevant to LEDs) the thermalization length is much smaller than the contact region with the latter comprising a sizeable fraction ($\sim$10%) of the device. Based on the above discussion we conclude that the contact region should be treated in an explicit manner and that it may be treated under the premise of drift–diffusion models.
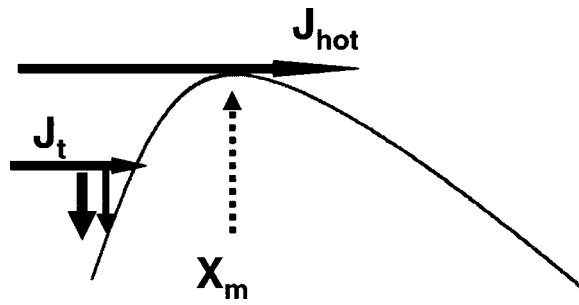
---

[a]Electronic mail: nir@ee.technion.ac.il

FIG. 1. Schematic of the contact region. x_m is the coordinate of peak of the image force potential in the presence of an applied field, J_t is the current of carriers thermalized at the contact region, J_h is the current of "hot" carriers that successfully overcome the peak ballistically.

III. DEVICE MODELS

A. Space charge limited current

The upper bound for the current flowing through any undoped device is given by the so-called space charge limited current (SCLC) relation (bulk limited):

$$J_{SCL} = \frac{9}{8} \varepsilon \varepsilon_0 \mu \frac{V^2}{L^3}. \tag{3}$$

B. Emission diffusion (generalized SCLC)

While expression (3) is valid for low barrier injection contacts it can be extended to include contact-limiting effects using the following formulas:[1]

$$J_{ED} = q N_0 \mu E(0) \exp\left(-\frac{q\phi_b}{kT}\right),$$
$$\phi_b = \phi_{b0} - \sqrt{\frac{qE(0)}{4\pi\varepsilon\varepsilon_0}}, \tag{4}$$

where Φ_b is the potential value at its maximum (point x_m in Fig. 1). The drop in voltage between x_m and the other contact ($x = L$) is then given by

$$V_{ED} = \int_0^L \sqrt{E^2(0) + \frac{2Jx}{\mu\varepsilon\varepsilon_0}} dx. \tag{5}$$

The physical picture of this model is transport of charge carriers under the combined (joint) potential of the image force lowered by the potential applied (see Fig. 1). If the initial concentration of the carriers at the lower point of potential, at the metallurgic junction, is equal to the total DOS (N_0) then the concentration at the top of the potential (x_m) is given by

$$n(x_m) = N_0 \exp\left(-\frac{q\phi_b}{kT}\right). \tag{6}$$

At x_m the current is assumed to be drift current only and proportional to $n(x_m)E(x_m)$, where one assumes that $x_m \approx 0$ or $E(0) \approx E(x_m)$. Due to this latter assumption, the influence of space charge on the value of voltage applied is taken into account only beyond the contact region ($x > x_m$) and the high charge density at the metal/semiconductor interface is neglected (since the contact region is lumped into a single point). When applied to single carrier devices the semianalytical model shown above [Eqs. (3)–(5)] is similar to the "standard" numerical semiconductor device models.[7–9]

C. Explicit model

1. Semiconductor device model

In this article we present results obtained by self-consistent solution of an explicit model and compare its results to widely used models for charge injection.

The equations that constitute the model are

$$-D\partial n/\partial x - \mu n \partial\phi/\partial x = J, \tag{7}$$
$$\phi = \phi_{SC} + \phi_{image} + \phi_{applied}, \tag{8}$$
$$\partial^2\phi_{SC}(x)/\partial x^2 = q/(\varepsilon\varepsilon_0), \tag{9}$$
$$\phi_{image}(x) = -q/(8\pi\varepsilon\varepsilon_0 x) + \phi_{barrier}, \tag{10}$$

where n is the charge density, D is the diffusivity constant, μ is the mobility, ϕ_{SC} is the potential induced by the spatial distribution of charge carriers, ϕ_{image} is the image force potential at the contact, and ϕ is the total potential experienced by the carriers. We compare this model to three other models. To make the comparison simpler we do not account for the field dependence of the mobility.[9]

Our numerical simulation is based on solving Eq. (7) using the exponentially fitted finite difference solution method as outlined in Refs. 20 and 21 and in the Appendix. To illustrate the actual effect of lumping the contact region into a single point in space [Eqs. (4) and (6)] we plot in Fig. 2 the electronic potential calculated by "standard" (lumped-contact) models[7–9] along results obtained using the explicit model presented here. In these calculations the device length is assumed to be 100 nm, the total DOS $N_0 = 10^{20}$ cm^{-3}, the mobility $\mu = 10^{-6}$ cm^2 V^{-1} s^{-1}, and the contact barrier is 0.2 and 0.3 eV for Figs. 2(A) and 2(B), respectively. The dashed line corresponds to lumped-contact model[7–9] results and the solid line to results obtained through the explicit model described here. We note that in the lumped-contact models a sizeable region, between $x = 0$ and x_m, is pushed out of the device (pushed to the left in Fig. 2).

In order to examine the change in physical picture induced by neglect of the contact region we plot in Fig. 3 the charge distribution calculated for devices having the same contact barriers as those in Fig. 2 and operated at a net applied voltage ($V_{appl} - V_{bi}$) of 0.5 V. Figure 3 illustrates a few points. First, for an injection barrier of 0.2 eV there is agreement regarding the predicted charge density at the bulk hence one would expect a similar $I - V$ relation (bulk limited). Second, for the injection barrier above 0.2 eV (see 0.3 eV) the lumped-contact model tends to overestimate the voltage-induced barrier lowering, resulting in a significantly higher charge density in the bulk (hence higher currents). Third, even for cases where the injection-contact barrier plays a role the image force still induces a high charge density close to the contact (metal/polymer) interface, as calculated by the explicit model. Neglect of this high-density region of 5–10 nm and of its space charge is the reason for overestimation of the voltage-induced barrier lowering.[22] It
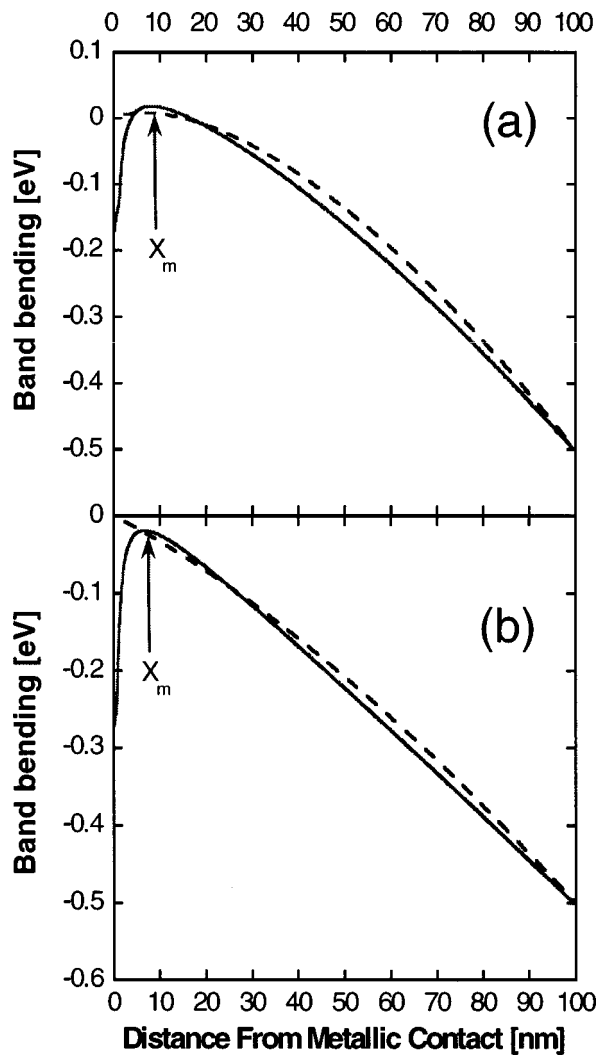
FIG. 2. Typical band bending. The barrier heights are (a) 0.2 and (b) 0.3 eV, respectively. The voltage applied is 0.5 V beyond the flat band condition (i.e., $V \sim 2.5$ V). The dashed line was calculated using the "standard" (lumped) model and the solid line using our explicit model.

FIG. 3. Charge density distribution for contact injection barriers of (a) 0.2 and (b) 0.3 eV. The dashed line was calculated using the "standard" (lumped) model and the solid line using our explicit model.

is also interesting to note that in order to account for high charge density at the interface there is no need to invoke extrinsic traps or defects.

The above effects also manifest themselves in the $I-V$ characteristics of the device. Figure 4(A) compares simulation results of current–voltage device characteristics to those of the (semí) analytical predictions (lumped-contact models). As expected, for low injection-barrier cases, the SCLC model is a reasonable approximation and for the 0.2 eV barrier all three models effectively converge. For higher injection barriers, like 0.4 eV, the role of the contact region has to be explicitly taken into account, especially when low voltages are applied. At high voltages the main drawback of the lumped models (standard) is that they tend to overestimate the voltage-induced barrier lowering effect, resulting in overestimation of the charge density in the bulk and hence of the current density. This is shown clearly in Fig. 4(B) which presents, on a linear scale, the $I-V$ curves for the 0.6 eV barrier case.
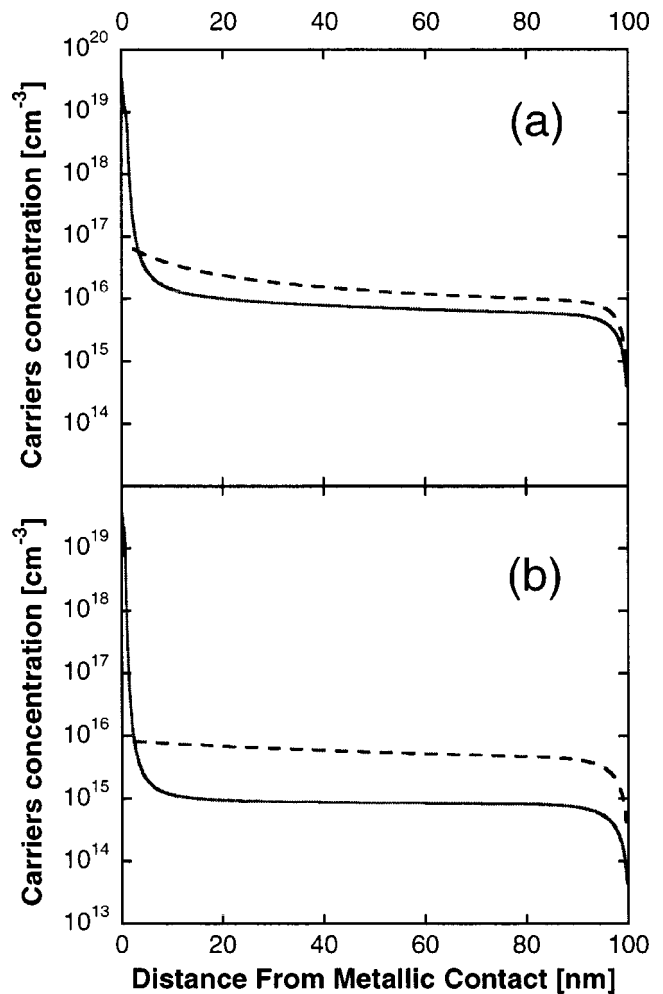
2. Accounting for the Gaussian DOS

The advantage of the explicit model described here is that once contact is made part of the transport equations it becomes possible to account for unique properties associated with organic materials. The most common property is that of disorder and the Gaussian distribution of the DOS.[4] It has recently been shown that within the framework of the semiconductor transport equation the Gaussian DOS results in the mobility (μ) and diffusivity (D) not being related through the classical Einstein relation $(D/\mu = kT/q)$ but rather through a generalized relation of the form of $D/\mu = \eta \cdot kT/q$ [23] where η is a function of both the charge density (n) and the width of the Gaussian DOS (σ) (see Fig. 5). The main assumption in this calculation is that of equilibrium, which has not been fully proved. However, such an assumption is embedded in most device models and in the case at hand the final result is in good agreement with Monte-Carlo simulations.[15,24] More details on the derivation of the generalized Einstein relation can be found in Ref. 23. Note that η is strongly dependent on the disorder parameter especially at high charge densities, i.e., this phenomenon should affect transport in the contact region $(0 < x < x_m)$ where the density is high (see Fig. 3).
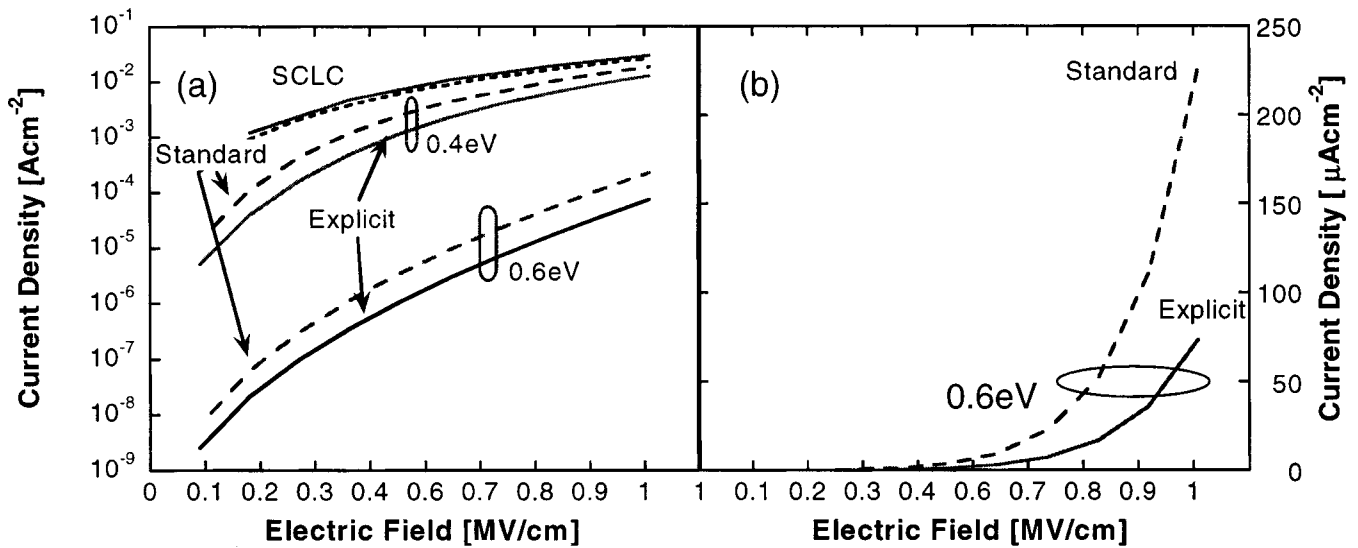
FIG. 4. (a) Current density as a function of the mean field for a 100 nm long device and varying injection barriers of 0.2, 0.4, and 0.6 eV and device length of 0.1 μm. (b) Current density for a 0.6 eV barrier on a linear scale. Standard = Lumped model; explicit = our model; SCLC = space charge limited current as in Eq. (3).

Mathematically speaking, one should find the self-consistent solution of the following, slightly modified, continuity equation:

$$-\eta(n,\sigma)\frac{kT}{q}\mu\,\partial n/\partial x - \mu n\,\partial\phi/\partial x = J. \qquad (11)$$

Accounting for $\eta_{(n)}$ requires modification of the numerical method. For a fine enough grid, one in which the density (n) does not change by more than an order of magnitude between successive grid points, one can still make use of the exponentially fitted finite difference scheme.[20,21] In this case accounting for $\eta_{(n)}$ in the numerical code is made trivial (see the Appendix). Figure 6 shows the calculated charge density distribution for several disorder parameters (σ). In the calcu-

lation the difference in energy between the Gaussian center and the metal work function is fixed at 0.5 eV and the net voltage applied $(V-V_{bi})$ is 2 V. As the Gaussian width is made larger more transport states become available close to the energy of the metal work function and hence the injection barrier effectively becomes smaller.[15,24] Figure 7 shows the calculated current–voltage relations for the cases shown in Fig. 6. The dependence of the mobility (μ) on the disorder (σ) is not included and hence only the functional form of the curves is important. One should keep in mind that disorder also reduces the mobility and hence the curves in Fig. 7 would shift slightly downward $\{\mu\propto\exp([(-2/3\sigma)^2])\}^4$. As expected, Fig. 7 shows that as σ is made larger, for a fixed difference in energy between the Gaussian center and the metal, the $I-V$ curve tends towards the SCLC functional form. This is consistent with the reduction of the effective barrier discussed with in the context of Fig. 6.
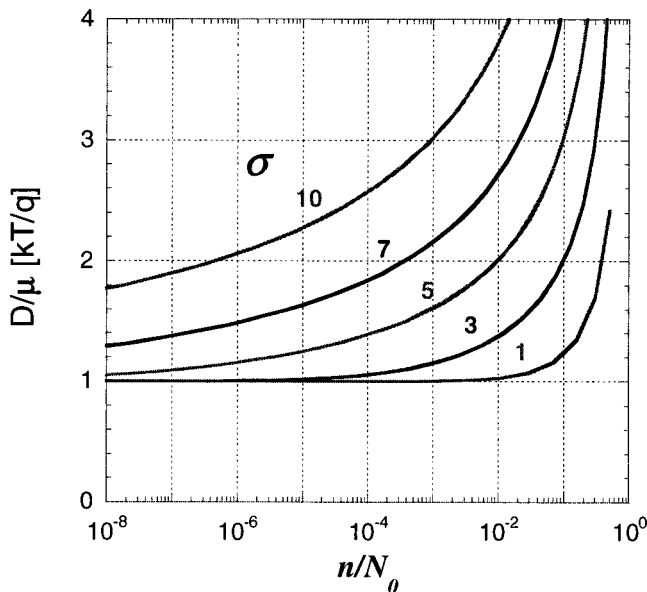

FIG. 5. Generalized Einstein relation (η) as a function of the charge concentration for a variety of disorder parameters (calculated based on Ref. 23); N_0 is the total DOS.
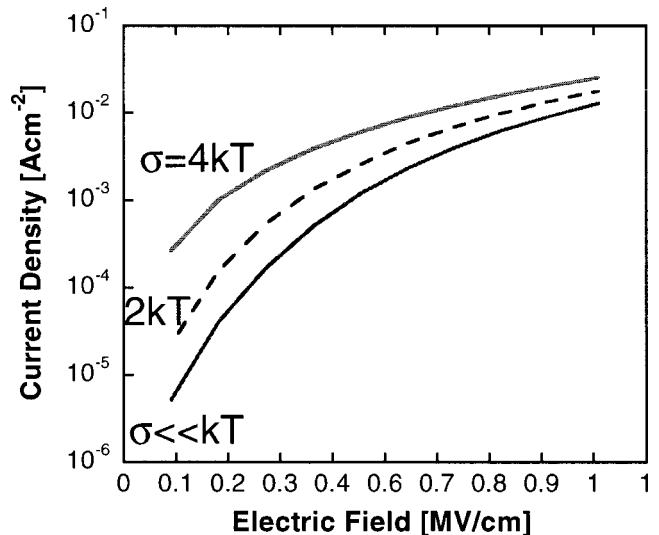

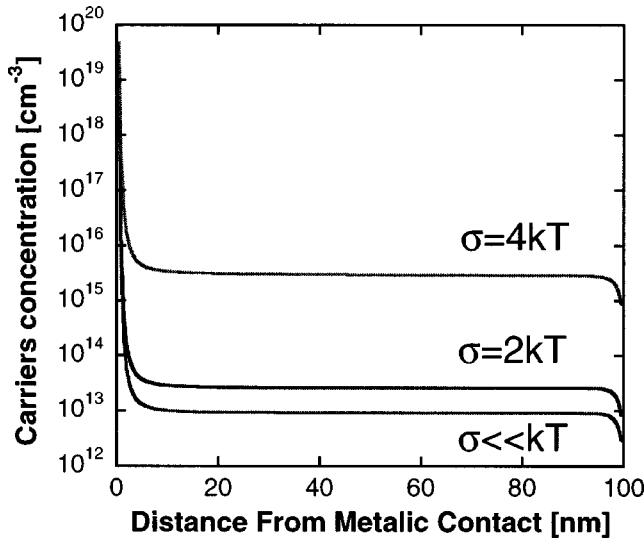
FIG. 6. Charge density distribution.

FIG. 7. Influence of disorder on device behavior. The charge distribution and $I-V$ curve show a significant variety for difference disorder in hopping site energies.

IV. CONCLUSIONS

We have presented a self-consistent analysis of charge injection and transport in low mobility disordered materials. It was found that incorporating the contact region into the transport model is important to properly account for contact phenomena. The model shows that a high charge density near the metallic interface is due to the image-force potential and does not require the addition of extrinsic trap states or defects. Moreover, it makes it possible to account for unique features associated with organic materials, like disorder and Gaussian DOS which are known to affect the injection process, all within the framework of a conventional semiconductor device model. We emphasize that all these effects enter the model through a single parameter, η,[23] and hence can be added to any semiconductor device model simulator (see the Appendix). We expect that the method described here will make it possible to better simulate, design, and manufacture state-of-the-art LEDs that can operate at low voltages and potentially have a fast switching time.

ACKNOWLEDGMENTS

APPENDIX: DISCRETIZATION OF THE CONTINUITY EQUATION

The simulation program solves the continuity equation

$$D \frac{\partial n}{\partial x} + \mu n \frac{\partial \phi}{\partial x} = J,$$

where $\Phi(x)$ is a joint potential of space charge induced field, the image potential near the contact, and the voltage applied. The charge carriers are assumed to be thermalized at the first hop so one can assume the concentration in the vicinity of the metallurgic junction to be in equilibrium with metal electrons. If $\Phi(x)$ and J are known one can derive an analytical solution of continuity equation for carrier concentration:

$$n(x) = N_0 \exp\left(-\frac{\mu}{D} \phi(x) \right) - \frac{J}{D} \exp\left(-\frac{\mu}{D} \phi(x) \right)$$

$$\times \int_0^x \exp\left(\frac{\mu}{D} \phi(x') \right) dx'.$$

The above representation clearly shows the importance of the ration μ/D. For the numerical solution we apply a discretization scheme:

$$n_i = n_{i-1} \exp\left(-\frac{\mu}{D}(\phi_i - \phi_{i-1}) \right) - \frac{J}{D}$$

$$\times \exp\left(-\frac{\mu}{D}(\phi_i - \phi_{i-1}) \right) \int_{x_{i-1}}^{x_i} \exp\left(\frac{\mu}{D} \phi(x') \right) dx'.$$

By writing an analogous expression for the next mesh interval and expressing J through $n(x)$ one can arrive at a scheme that contains the carrier concentration only:

$$J = D \left[\frac{n_{i-1} - n_i \exp\left(\frac{\mu}{D}(\phi_i - \phi_{i-1}) \right)}{\int_{x_{i-1}}^{x_i} \exp\left(\frac{\mu}{D} \phi(x') \right) dx'} \right]$$

$$= D \left[\frac{n_i - n_{i+1} \exp\left(\frac{\mu}{D}(\phi_{i+1} - \phi_i) \right)}{\int_{x_i}^{x_{i+1}} \exp\left(\frac{\mu}{D} \phi(x') \right) dx'} \right].$$

By rearranging terms when assuming $\mu/D = q/kT$ we arrive at the following discretization scheme:[20,21]

$$\frac{n_{i-1}}{\int_{x_{i-1}}^{x_i} \exp\left(\frac{q}{kT} \phi(x') \right) dx'}$$

$$- n_i \left[\frac{\exp\left(\frac{q}{kT}(\phi_i - \phi_{i-1}) \right)}{\int_{x_{i-1}}^{x_i} \exp\left(\frac{q}{kT} \phi(x') \right) dx'} \right.$$

$$\left. + \frac{n_i}{\int_{x_i}^{x_{i+1}} \exp\left(\frac{q}{kT} \phi(x') \right) dx'} \right]$$

$$+ \frac{n_{i+1} \exp\left(\frac{q}{kT}(\phi_{i+1} - \phi_i) \right)}{\int_{x_i}^{x_{i+1}} \exp\left(\frac{q}{kT} \phi(x') \right) dx'} = 0.$$

In the generalized Einstein relation case $\mu/D = q/\eta kT$ and hence the discretization scheme is written as

$$\frac{n_{i-1}}{\int_{x_{i-1}}^{x_i} \exp\left(\frac{q}{\eta_{i-1/2}kT}\phi(x')\right)dx'}\eta_{i-1/2}$$

$$-n_i\left[\frac{\exp\left(\frac{q}{\eta_{i-1/2}kT}(\phi_i-\phi_{i-1})\right)}{\int_{x_{i-1}}^{x_i}\exp\left(\frac{q}{\eta_{i-1/2}kT}\phi(x')\right)dx'}\eta_{i-1/2},\right.$$

$$\left.+\cdots\frac{n_i}{\int_{x_i}^{x_{i+1}}\exp\left(\frac{q}{\eta_{i+1/2}kT}\phi(x')\right)dx'}\eta_{i+1/2}\right]$$

$$+\frac{n_{i+1}\exp\left(\frac{q}{\eta_{i+1/2}kT}(\phi_{i+1}-\phi_i)\right)}{\int_{x_i}^{x_{i+1}}\exp\left(\frac{q}{\eta_{i+1/2}kT}\phi(x')\right)dx'}=0.$$

The above scheme is valid only for a fine enough grid so that η can be assumed to be constant between the mesh points (namely, the difference incharge density between adjacent points is below a factor of 3).

For any given electronic potential distribution the equation above can be solved and yield the charge distribution. To account for the self-induced potential (space charge effects) we also solve the Poisson equation in a self-consistent manner. The algorithm is based on an iterative solution until solution convergence is achieved.

[1] N. F. Mott and R. W. Gurney, Electronic Processes in Ionic Crystals (Oxford University Press, London, 1940).
[2] M. Pope and C. E. Swenberg, Electronic Processes in Organic Crystals (Clarendon P, Oxford, UK, 1982).
[3] R. H. Friend et al., Nature (London) **397**, 121 (1999).
[4] M. Van der Auweraer, F. C. Deschryver, P. M. Borsenberger, and H. Bassler, Adv. Mater. **6**, 199 (1994).
[5] H. Scher, M. F. Shlesinger, and J. T. Bendler, Phys. Today **44**, 26 (1991).
[6] E. M. Conwell and M. W. Wu, Appl. Phys. Lett. **70**, 1867 (1997).
[7] G. G. Malliaras and J. C. Scott, J. Appl. Phys. **85**, 7426 (1999).
[8] P. S. Davids, I. H. Campbell, and D. L. Smith, J. Appl. Phys. **82**, 6319 (1997).
[9] D. J. Pinner, R. H. Friend, and N. Tessler, J. Appl. Phys. **86**, 5116 (1999).
[10] A. J. Campbell, D. D. C. Bradley, H. Antoniadis, M. Inbasekaran, W. S. W. Wu, and E. P. Woo, Appl. Phys. Lett. **76**, 1734 (2000).
[11] A. Kraft, G. A.C., and H. A.B., Angew. Chem. Int. Ed. Engl. **37**, 402 (1998).
[12] M. A. Baldo and S. R. Forrest, Phys. Rev. B **64**, 5201 (2001).
[13] J. M. Lupton, V. R. Nikitenko, I. D. W. Samuel, and H. Bassler, J. Appl. Phys. **89**, 311 (2001).
[14] J. C. Scott and G. G. Malliaras, Chem. Phys. Lett. **299**, 115 (1999).
[15] V. I. Arkhipov, U. Wolf, and H. Bassler, Phys. Rev. B **59**, 7514 (1999).
[16] E. Tutis, M. N. Bussac, B. Masenelli, M. Carrard, and L. Zuppiroli, J. Appl. Phys. **89**, 430 (2001).
[17] D. F. Blossey, Phys. Rev. B **9**, 5183 (1974).
[18] J. Mort, F. W. Schmidlin, and A. I. Lakatos, Appl. Phys. Lett. **42**, 5761 (1971).
[19] B. Masenelli, D. Berner, M. N. Bussac, F. Nuesch, and L. Zuppiroli, Appl. Phys. Lett. **79**, 4438 (2001).
[20] S. Selberherr, Analysis and Simulation of Semiconductor Devices (Springer, Wien, Germany, 1984).
[21] M. S. Mock, Analysis of Mathematical Models of Semiconductor Devices (Boole, Dublin, 1983).
[22] Y. Preezant, Y. Roichman, and N. Tessler, J. Phys.: Condens. Matter (to be published).
[23] Y. Roichman and N. Tessler, Appl. Phys. Lett. **80**, 1948 (2002).
[24] V. I. Arkhipov, E. V. Emelianova, Y. H. Tak, and H. Bassler, J. Appl. Phys. **84**, 848 (1998).